New Magnetic Order in Buried Native Iron Oxide Layers

G. S. D. Beach,[1,2,*] F. T. Parker,[1] David J. Smith,[3] P. A. Crozier,[3] and A. E. Berkowitz[1,2]

[1]*Center for Magnetic Recording Research, University of California, San Diego, La Jolla, California 92093-0401, USA*
[2]*Department of Physics, University of California, San Diego, La Jolla, California 92093-0354, USA*
[3]*Center for Solid State Science and Department of Physics and Astronomy, Arizona State University, Tempe, Arizona 85287-1504, USA*

(Received 9 May 2003; published 23 December 2003)

The properties of a magnetically ordered buried Fe oxide layer are presented. This oxide has a room-temperature magnetization exceeding that of Fe_3O_4 by 42% and of γ-Fe_2O_3 by 89%. The oxide consists of a component (70%) with a net moment of $2.0\mu_B$/Fe ion, while the remaining spins yield no net moment. The oxide magnetization is stabilized in part by the proximate Fe metal.

DOI: 10.1103/PhysRevLett.91.267201 PACS numbers: 75.25.+z, 75.70.Cn, 76.80.+y

Surface and interface effects in ultrathin native Fe oxide layers often lead to spin configurations not observed in the bulk. The bulk Fe oxides include the classical antiferromagnet FeO, α-Fe_2O_3, an antiferromagnet with a small parasitic moment, and ferrimagnetic γ-Fe_2O_3 and Fe_3O_4, in which a substantial net moment exists due to the unequal moments of two antiparallel sublattices. By contrast, spin-glass-like frustration has been observed in the native oxides formed on passivated Fe particles [1–3] and thin films [4], as well as on the surface of oxide nanoparticles [5,6]. More surprising, *ferromagnetic* order in native Fe oxides has been reported by several authors [7,8]. The possibility of enhanced net moment in Fe oxides is of particular importance due to the large ionic moments of Fe^{2+} ($4\mu_B$) and Fe^{3+} ($5\mu_B$). The magnetization of ferromagnetic FeO [8], for example, would exceed that of metallic Fe. However, the quantitative measurement of an enhanced net moment in an Fe oxide has heretofore not been presented.

We report a *buried* native Fe oxide with the largest magnetization yet observed in any Fe oxide system, exceeding that of Fe_3O_4 by 42% and of γ-Fe_2O_3 by 89%. The native oxide, formed in a metal/native oxide multilayer (MNOM) structure, contains a distinct magnetic component having a net moment with magnitude and temperature dependence comparable to those of metallic Fe. This large net moment is present in an oxide with a stoichiometry near FeO, and is stabilized in part through close proximity with the metal.

Fe MNOMs were fabricated at room temperature via sputter deposition [9]. These polycrystalline samples were deposited on Si(100) substrates except where noted. The notation $[\mathrm{Fe}(t_0)/\mathrm{oxide}]_N$ describes a MNOM with N unit bilayers, each consisting of a nominal thickness t_0 of Fe which has been exposed *in situ* to oxygen ($\sim 8 \times 10^{-5}$ Torr) for 10 s. A final 100 Å SiO_2 cap prevented further oxidation. Samples with t_0 ranging from 5 to 60 Å were prepared, with $N \geq 30$ and $Nt_0 \gtrsim 1000$ Å.

The cross-sectional electron micrograph of Fig. 1 depicts the MNOM microstructure for $t_0 = 20$ Å. The oxide and metal layers are visible as horizontal regions of light and dark contrast, respectively. Lattice fringes in both metal and oxide are visible, and show the polycrystallinity of each layer. In some regions, lattice fringes across multiple layers are resolved, indicating locally epitaxial metal/oxide and oxide/metal growth.

Room-temperature conversion electron Mössbauer spectroscopy (CEMS) was used to characterize each MNOM. The temperature (T) dependence was studied for a representative $t_0 = 20$ Å MNOM on a kapton substrate using transmission Mössbauer spectroscopy (TMS). No differences were found between the room-temperature TMS spectrum [Fig. 2(a)] and the CEMS spectra of similar MNOMs on Si. All spectra were consistently fitted to a model of metal (Fe^0) and oxide sextets, distinguished via isomer shift (IS). The oxide component was fitted with a discrete set of subspectra with equally spaced hyperfine fields (HFs), as described below. Two sextets were used to account for an asymmetric broadening in the Fe^0 subspectrum [4]. Fits yield a HF of 330 kOe and IS of 0.00 mm/s for one sextet, indicative of bulk α-Fe. The relative area of the second Fe^0 sextet corresponds to a constant 1.8(1) Å per interface for all t_0, with an "interfacially" enhanced [4] HF ($\sim$350 kOe) and

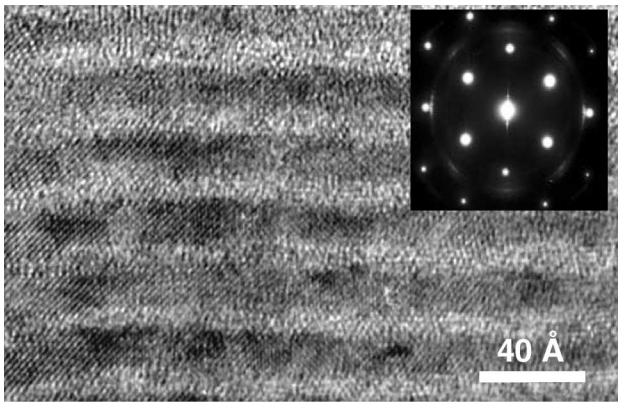

FIG. 1. Cross-sectional high-resolution electron micrograph for $[\mathrm{Fe}(20\ \text{Å})/\mathrm{oxide}]_{50}$. Inset: Electron diffraction pattern showing MNOM texture relative to Si(100) substrate.

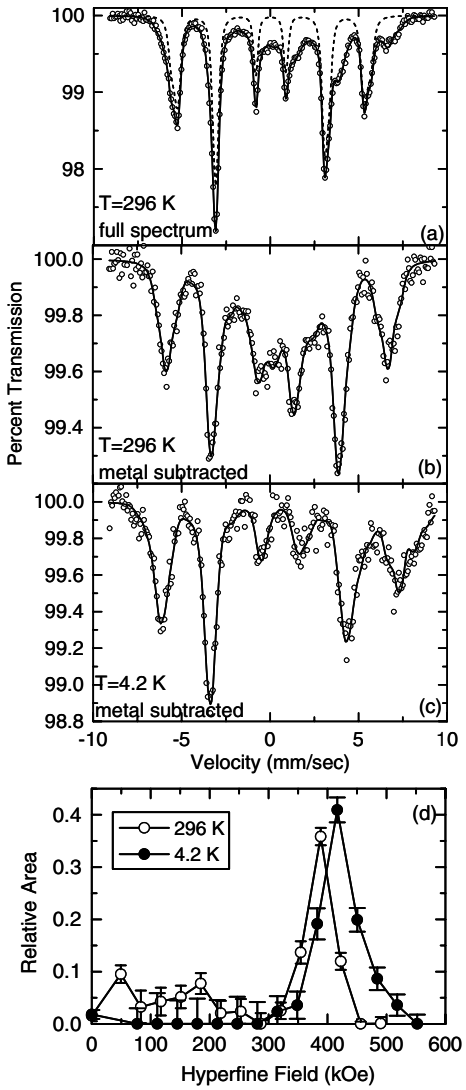

FIG. 2. (a) Transmission Mössbauer spectrum for $[\mathrm{Fe}(20\ \text{Å})/\mathrm{oxide}]_{50}$ on kapton at 296 K, with full fit (solid line) and metal subspectrum fit (dashed line). Spectra with the fitted metal subspectrum subtracted are shown for (b) 296 K and (c) 4.2 K, in which solid lines are subfits corresponding to the oxide hyperfine field distributions of (d).

IS ($\sim$0.05 mm/s). The fits give line intensity ratios $3{:}2p{:}1{:}1{:}2p{:}3$ with $p \approx 2$ for both the metal and the oxide, implying in-plane moments. The fraction f of Fe as Fe^0, proportional to the relative area of the Fe^0 subspectrum, gives the nominal thickness t_{ox} of Fe that oxidizes per layer, $t_{\mathrm{ox}} = (1 - f)t_0$. t_{ox} is independent of t_0 and averages 8.4(2) Å for all samples, consistent with TEM.

The net moment $\overline{\mu}_{\mathrm{net}}$ of a MNOM is the sum of the net moments of the metal (μ^m_{net}) and oxide ($\mu^{\mathrm{ox}}_{\mathrm{net}}$), weighted by their respective fractions, and may be written $\overline{\mu}_{\mathrm{net}} = \mu^{\mathrm{ox}}_{\mathrm{net}} + (\mu^m_{\mathrm{net}} - \mu^{\mathrm{ox}}_{\mathrm{net}})f$. A linear relation between $\overline{\mu}_{\mathrm{net}}$ and f may be used to independently determine μ^m_{net} and $\mu^{\mathrm{ox}}_{\mathrm{net}}$. Figure 3 shows that $\overline{\mu}_{\mathrm{net}}$, measured at 300 K using a SQUID magnetometer, is linear with f for $f \gtrsim 0.40$ ($t_0 \gtrsim 14$ Å), giving net moments of $2.1(1)\mu_B$/Fe and $1.38(6)\mu_B$/Fe for the metal and oxide, respectively. μ^m_{net} agrees with that of bulk α-Fe, $2.172\mu_B$/Fe. Nearly identical data are found at 5 K, with both μ^m_{net} and $\mu^{\mathrm{ox}}_{\mathrm{net}}$ increasing by only $\sim$2%.

The T dependence of the oxide ionic moment, proportional to that of the HF, reveals two magnetic components in the oxide. The TMS oxide subspectrum at 296 K is shown in Fig. 2(b), where the fitted Fe^0 contribution has been subtracted. The oxide subspectrum consists of a relatively sharp magnetically split sextet and a broad parabolic background, with the latter shifted towards positive velocity with respect to the former. The fit results from the hyperfine field distribution (HFD) are shown in Fig. 2(d). The three main subspectra of the HFD, centered at 387 kOe, fit the main oxide sextet. The remaining lower HF subspectra, with an average HF of $\sim$140 kOe, account for the broad component. Nearly identical oxide subspectra, with the main sextet comprising 70(2)% of the oxide spectrum, are found with CEMS for all MNOMs having $t_0 > 14$ Å.

The main sextet shows little change with decreasing T, while the HF splitting of the broad component increases continuously. In the oxide subspectrum at 4.2 K, shown in Fig. 2(c), the broad component has split out fully, overlapping with the main sextet and causing the asymmetry of the spectrum due to its larger IS. This is reflected in the HFD [Fig. 2(d)], where the area shifts from the low HF subspectra to those with HFs larger than that of the main sextet. The contrasting T dependence of the HFs of the two spectral components, quantified by the corresponding HFDs, indicates that they represent two magnetic components in the oxide. The majority component, giving rise to the weakly T-dependent main sextet, consists of ordered sites stabilized by a strong exchange field. The remaining minority oxide component shows no change in room-temperature splitting in fields up to 3 kOe, precluding superparamagnetism [10]. Rather, the strong T dependence and broad high-T distribution of the HFs of the minority component suggest ionic sites with a range of weak exchange fields.

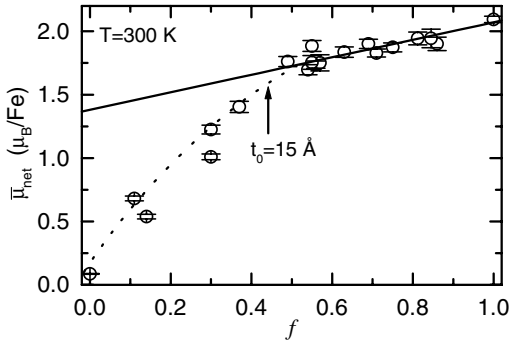

FIG. 3. Saturation moment at 300 K versus metal fraction for $[\mathrm{Fe}(t_0)/\mathrm{oxide}]_N$. The solid line is a linear fit to the data with $f > 0.40$, the dotted line is a visual guide.

$\mu_{\rm net}^{\rm ox}$ determined from Fig. 3 is the *average* of the net moments of the majority ($\mu_{\rm net}^{\rm ox'}$) and minority ($\mu_{\rm net}^{\rm ox''}$) oxide components, given by $\overline{\mu}_{\rm net}^{\rm ox} = 0.70\mu_{\rm net}^{\rm ox'} + 0.30\mu_{\rm net}^{\rm ox''}$ based on their relative fractions. Although $\overline{\mu}_{\rm net}^{\rm ox}$ decreases by only $\sim$2% from 5 to 300 K, the average HF, and thus the ionic moment, of the *minority* oxide component shows a fourfold decrease at 296 K. Thus the spins of the minority component contribute negligibly to the *net* moment. The observed T dependence of $\mu_{\rm net}^{\rm ox}$ and the average HF limits $\mu_{\rm net}^{\rm ox''}$ to $0.00(8)\mu_B$/Fe at 300 K, suggesting an antiferromagnetic or a frozen canted spin structure for this component. This leaves the majority component responsible for the entire net moment: $\mu_{\rm net}^{\rm ox'} = 2.0(1)\mu_B$/Fe at 300 K. Considering the saturation ionic moments of Fe^{2+} ($4.0\mu_B$) and Fe^{3+} ($5.0\mu_B$), a net moment of $2.0\mu_B$/Fe suggests ferrimagnetic order in the majority component with 70%–75% of the spins, depending on valence, parallel to the net moment and the remainder antiparallel. The net moment of the majority component is much larger than the $1.15\mu_B$/Fe and $1.37\mu_B$/Fe found in γ-Fe_2O_3 and Fe_3O_4, respectively, and is comparable in its magnitude and T dependence to that of α-Fe.

Although the magnetic moment of the native oxide suggests a comparison with the spinel oxides, bulk-density Fe_3O_4 or γ-Fe_2O_3 should occupy $\sim$2/3 of the volume of $[\text{Fe}(20\ \text{Å})/\text{oxide}]_{50}$, based on the metal fraction. This appears inconsistent with the electron micrograph of Fig. 1. The inconsistency is quantified by considering the minimum volume required by a metal/oxide composite given the metal fraction. In $[\text{Fe}(t_0)/\text{oxide}]_N$, the metal/native oxide bilayer thickness Λ is larger than t_0 due to the oxidation and subsequent expansion of a fraction $(1 - f)$ of the Fe by a factor α. In each bilayer, a *nominal* thickness $t_{\rm ox} = (1 - f)t_0$ of Fe oxidizes, leaving a metal layer of nominal thickness $t_m = ft_0$. With $\Lambda = t_m + \alpha t_{\rm ox}$, the total expansion of a MNOM, Λ/t_0, is determined solely by α and f via $\Lambda/t_0 = \alpha + (1 - \alpha)f$.

X-ray reflectivity (XRR) accurately yields the total MNOM thickness $N\Lambda$ or, equivalently, Λ. In Fig. 4, Λ/t_0 versus f for a series of MNOMs falls on a single line of constant $\alpha = 1.51(4)$. This is compared with the values 1.7, 2.10, 2.13, and 2.33 for bulk FeO, Fe_3O_4, α-Fe_2O_3, and γ-Fe_2O_3, respectively. Because the ionic volume of O^{2-} is $\sim$10–20 times greater than those of Fe^{2+} and Fe^{3+} [11], the oxidized Fe expansion depends only on the quantity and packing density of the incorporated O^{2-}. In the bulk Fe oxides, the O^{2-} forms a close packed (fcc or hcp) lattice with the much smaller Fe ions in interstitial sites. The O^{2-} packing density cannot be increased significantly from what is found in the bulk. The small expansion of the MNOM is therefore inconsistent with the incorporation of any more than $\sim$1 O^{2-} ion per Fe ion. To accommodate the O^{2-} required for an Fe^{3+} oxide in $[\text{Fe}(20\ \text{Å})/\text{oxide}]_{50}$, for example, would require a total thickness greater by $\sim$350 Å than the 1200 Å measured by XRR. Thus we may conclude that the native oxide is predominantly Fe^{2+}.

Fe^{2+} is confirmed by electron energy loss spectroscopy (EELS). An EELS microprobe ($\sim$1 nm width) was scanned along a cross-sectioned $[\text{Fe}(20\ \text{Å})/\text{oxide}]_{50}$ sample, shown in Fig. 5(a). Using suitable calibration standards, the ratio of the integrated O K edge to the Fe L_{23} edge as a function of position gives the O/Fe profile shown in Fig. 5(b). The data were modeled by convolving a step-profile composition model of variable O/Fe ratio with an appropriate probe function [12]. The fit was optimized over the three central bilayers, with the discrepancy at either end caused by thickness variations in the cross-sectioned sample. Fitted O/Fe ratios of 1.1 and 0.1 were obtained for the oxide and metal layers,

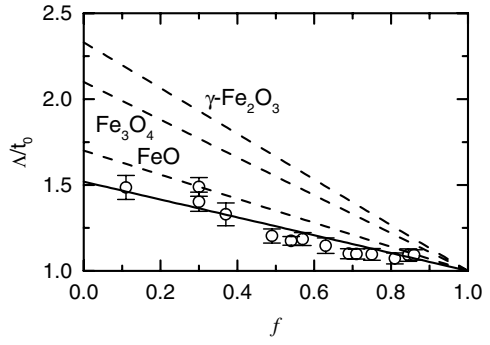

FIG. 4. Total volume expansion due to oxidation in $[\text{Fe}(t_0)/\text{oxide}]_N$ versus metal fraction. The solid line is a linear fit (see text). The dotted lines indicate the expansion required for the formation of the indicated oxide phases.

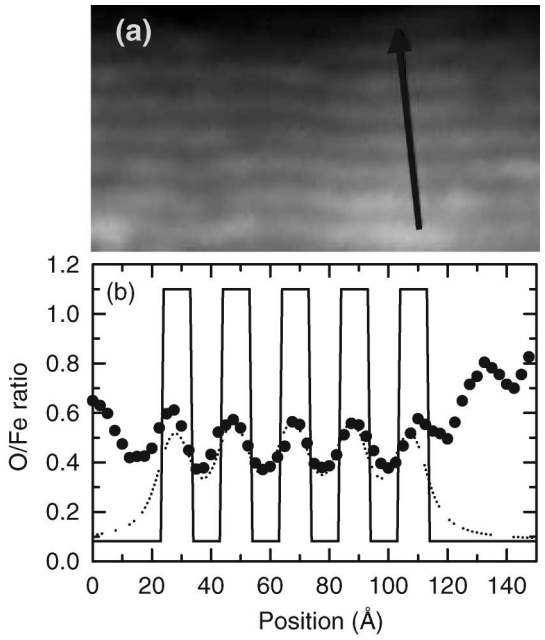

FIG. 5. (a) Annular dark-field cross-sectional electron micrograph of $[\text{Fe}(20\ \text{Å})/\text{oxide}]_{50}$ showing path of EELS probe. (b) O/Fe ratio along line scan for model profile (solid curve) convolved profile (dotted curve) and experimental points (filled circles).

respectively, with the nonzero oxygen content in the metal layers likely due to adsorbed oxygen on the cross-sectioned sample [12]. The results confirm a predominance of Fe^{2+} in the native oxide.

The average HF of the native oxide is consistent with the 400–450 kOe typical of ordered Fe^{2+}, and is much lower than the ~500–550 kOe of Fe^{3+}. However, the IS is typically $\gtrsim 1.0$ mm/s for Fe^{2+} and ~0.3–0.4 mm/s for Fe^{3+}. In comparison, the average IS of 0.37 mm/s and 0.65 mm/s for the majority and minority oxide components, respectively, at 296 K, suggest an average valence closer to Fe^{3+}. Changes in the HF and IS are known to accompany perturbations of the electronic structure at surfaces and interfaces. Considering the predominantly interfacial nature of the ultrathin buried oxide, the magnetic and electronic influence of the metal may be substantial. As f falls below ~0.4 ($t_m \sim 6$ Å), the majority oxide subspectrum collapses into a nonmagnetic doublet, causing the rapid fall off of $\overline{\mu}_{\text{net}}$ in Fig. 3. However, from Fig. 4, there is no evidence for a significant change in stoichiometry corresponding with the loss of magnetism. Thus, the metal *supports* the magnetism of the oxide. The loss of magnetism, and presumably metal/oxide exchange, is accompanied by an increase in the average oxide IS to ~0.7 mm/s at 296 K. Metal/oxide exchange would involve overlap of the metal conduction electrons with the oxide ion orbitals, and could increase the electron density at the ionic nuclei and contribute to a significant reduction of the IS from bulk-coordinated values.

The structure of the native oxide may also play a role in the observed properties. The native oxide is somewhat more dense than bulk FeO, as implied by a smaller α. Studies of FeO under compression show an increase in the ordering temperature beyond room temperature with increasing density, and a concomitant decrease in IS by up to 40% [13]. Vacancies and defects are known to form complex ordered structures in $Fe_{1-x}O$ [14] which can lead to a variety of novel behaviors including a nonzero net moment [15]. The present buried native oxide may be particularly susceptible to structural perturbations. Several studies [16,17] indicate that oxidation under the present conditions leads to an Fe^{3+}-rich surface layer. The subsequent Fe^0 layer in the MNOM may partially reduce each initial surface oxide layer [18], converting Fe^{3+} to Fe^{2+}. This is consistent with our finding [19], using ^{57}Fe probe layers, that ~1/3 of the Fe in the buried native oxide comes from the metal deposited on top. Oxidation followed by partial reduction of an ultrathin oxide layer under (local) epitaxial constraints could lead to complex defect structures, making the buried native oxide layer intrinsically different from a surface oxide.

In conclusion, we report a buried native FeO-like oxide consisting of two magnetic components. The minority component, at 30%, has no net moment and a strongly T-dependent ionic moment. The majority component has a net moment of $2.0\mu_B$/Fe, comparable in magnitude and T dependence to that of metallic Fe. A consequence of the high oxide density is that despite the "dilution" of the average net moment by the minority oxide component, the volume-averaged magnetization remains large: $M_s =$ 732(35) emu/cc, 42(6)% larger than for Fe_3O_4,and 89(8)% larger than for γ-Fe_2O_3. Thus, the magnetization of the present native oxide exceeds that of any other Fe oxide system. Eliminating the minority component could further increase the net oxide moment by up to 43%. Furthermore, as the origin of the net moment of the majority component is not yet clear, $2.0\mu_B$/Fe may not be its upper limit. Understanding the spin structure may suggest ways to further increase the net polarization, bringing the net moment closer to the $4.0\mu_B$/Fe of Fe^{2+}. By using a MNOM structure, a considerable volume of such an oxide could be obtained, with significant technological implications.

This work was supported in part by the National Institute of Standards and Technology's Nanotechnology Initiative. We acknowledge use of facilities at the Center for High Resolution Electron Microscopy at Arizona State University.

*Electronic address: gbeach@physics.utexas.edu

[1] K. Haneda and A. H. Morrish, Surf. Sci. **77**, 584 (1978).
[2] S. Linderoth, M. D. Bentzon, and S. Mørup, Nucl. Instrum. Methods Phys. Res., Sect. B **76**, 173 (1993).
[3] F. T. Parker, F. E. Spada, T. J. Cox, and A. E. Berkowitz, J. Appl. Phys. **77**, 5853 (1995).
[4] T. Shinjo, T. Iwasaki, T. Shigematsu, and T. Takada, Jpn. J. Appl. Phys. **23**, 283 (1984).
[5] J. M. D. Coey, Phys. Rev. Lett. **27**, 1140 (1971).
[6] R. H. Kodama, A. E. Berkowitz, E. J. McNiff, and S. Foner, Phys. Rev. Lett. **77**, 394 (1996).
[7] F. Bødker, S. Mørup, and S. Linderoth, Phys. Rev. Lett. **72**, 282 (1994).
[8] K. Koike and T. Furukawa, Phys. Rev. Lett. **77**, 3921 (1996).
[9] G. S. D. Beach, A. E. Berkowitz, F. T. Parker, and D. J. Smith, Appl. Phys. Lett. **79**, 224 (2001).
[10] S. Mørup, J. Magn. Magn. Mater. **37**, 39 (1983).
[11] *CRC Handbook of Chemistry and Physics*, edited by D. R. Lide (CRC Press, Boca Raton, 2002), 83rd ed.
[12] P. A. Crozier, M. Catalano, and R. Cingolani, Ultramicroscopy **94**, 1 (2003).
[13] M. P. Pasternak *et al.*, Phys. Rev. Lett. **79**, 5046 (1997).
[14] H. Fjellvåg, F. Grønvold, S. Stølen, and B. Hauback, J. Solid State Chem. **124**, 52 (1996).
[15] D. V. Dimitrov *et al.*, J. Appl. Phys. **87**, 7022 (2000).
[16] P. Graat and M. A. J. Somers, Surf. Interface Anal. **26**, 773 (1998).
[17] S. J. Roosendaal, A. M. Vredenberg, and F. H. P. M. Habraken, Phys. Rev. Lett. **84**, 3366 (2000).
[18] T. J. Regan *et al.*, Phys. Rev. B **64**, 214422 (2001).
[19] G. S. D. Beach, Ph.D. thesis, University of California, San Diego, 2003.